ISSN NO. 2320-5407

Journal homepage: http://www.journalijar.com

INTERNATIONAL JOURNAL OF ADVANCED RESEARCH

RESEARCH ARTICLE

The characteristics of $ZnO-MnO_2-Bi_2O_3-Co_2O_3-TiO_2$-based varistor ceramics doped with Sb_2O_3 and/or Cr_2O_3

Osama A. Desouky[1] and Mostafa M.H. Khalil[2]

[1] Higher Institute of Engineering (BHIE), Bilbis, Sharqia, Egypt
[2] Chemistry Department, Faculty of Science, Ain Shams University, 11566 Abbassia, Cairo, Egypt

Manuscript Info

Manuscript History:

Received: 11 December 2014
Final Accepted: 25 January 2015
Published Online: February 2015

Key words:

ceramics, ZnO, varistor, non-linear current-voltage behavior, Cr_2O_3, microstructure

Corresponding Author

Osama A. Desouky

Abstract

The effect of Cr_2O_3 and Sb_2O_3 on the physical and electrical properties of $ZnO-MnO_2-Bi_2O_3-Co_2O_3-TiO_2$-based varistors ceramics were investigated in this work. The microstructure and electrical properties of varistors, which are composed of $ZnO-MnO_2-Bi_2O_3-Co_2O_3-TiO_2$-based varistors ceramics, were investigated in the range of (0.04 - 0.2) mol% Cr_2O_3 samples (B1 , B2 & B3) and 0.12 mol % of both Cr_2O_3 and Sb_2O_3 sample (Z1) or 0.12 mol% Cr_2O_3 and 0.06 mol% Sb_2O_3 (Z2). All samples exhibit non-linear current-voltage behavior. Addition of Bi_2O_3 in present of Co_2O_3, MnO_2, Sb_2O_3 and Cr_2O_3 lead better densification by minimizing the present of closed pores. Also maximum values of firing shrinkage were attained in specimens fired at 1220 ^oC for 2 hours. SEM of mix B1, shows two phase, ZnO grains and intergranular phase triple point, and TiO_2, Co_2O_3 and Cr_2O_3 go into solid solution in the ZnO grains. Also Bi-rich phase in the triple point and increase the presence of liquid phase (melt liquid phase) on the grain boundary. The relation between I and V for the different mixes show very good plateau in (I-V) relation.

INTRODUCTION

ZnO is a very promising material for semiconductor device applications [1–5]. It has a direct and wide band gap in the near-UV spectral region [6–10], and a large free-exciton binding energy [6–9] so that excitonic emission processes can persist at or even above room temperature [11, 12]. ZnO crystallizes in the wurtzite structure, the same as GaN, but, in contrast, ZnO is available as large bulk single crystals [11]. Its properties have been studied since the early days of semiconductor electronics [13], but the use of ZnO as a semiconductor in electronic devices has been hindered by the lack of control over its electrical conductivity: ZnO crystals are almost always n-type, the cause of which has been a matter of extensive debate and research [1–5]. The physical properties of ZnO crystals depend strongly on the concentration of native defects caused by the deviation from the stoichiometric composition [14–17]. Zinc oxide varistors are a polycrystalline structured material consisting of semiconducting zinc oxide crystals and a second phase located at the boundaries of the crystals. This second phase consists of a certain number of metallic oxides (Bi_2O_3,MnO, Sb_2O_3, etc.). Thus, a zinc oxide varistor consists of a large number of boundaries forming a series-parallel network of resistors and capacitors, appearing somewhat like a multifunction semiconductor. Their excellent nonlinearly and electrical characteristics arising out of the grain boundaries are mostly dependent on the micro structural uniformity [18] . Ceramic processing results in semiconducting ZnO grains, with intergranular bismuth-rich oxide phases. The non-linear current– voltage characteristics are governed by the interfaces between the ZnO grains. The voltage-dependent resistivity results from Schottky barriers at ZnO-ZnO boundaries, but the Bi-rich phases present at multiple grain junctions also have a significant effect on the overall

resistivity [19–21]. In pure Bi_2O_3, the a monoclinic structure is the stable room temperature polymorph; on heating a transforms at 730 ^{0}C to the oxygen ion conducting face centered cubic phase [22]. Often, in ceramic varistors at room temperature, the tetragonal Bi_2O_3 phase [23–25] is reported, but there are also reports of the cubic y and g phases, as well as the a monoclinic form [26–30]. Originally, it was thought that the ZnO grains in the microstructure were separated by a continuous amorphous bismuth oxide layer [31,32]. Fabrication of ZnO varistors follow standard ceramic techniques. ZnO and other constituents are mixed by milling in a ball mill and dried by spraying. The mixture is pressed to the desired shape usually disc like. The resulting pellets are sintered at high temperature (typically 1000–1400^{0}C) [33]. The four basic compounds formed are ZnO, spinel, phrochlore and bismuth-rich phases. The phrochlore disappears at high temperature forming spinel and Bi_2O_3 [34]. The observed current–voltage characteristics of a varistor are often empirically described by the power law relation:

$$J = C\,(E)^{\alpha}$$

Where J is the current density, E the applied electrical field, α the coefficient of non-linearity and C is the proportionality constant that is related with the microstructure [35]. The aim of this work is to report experimental results that the doping of Cr_2O_3 and Sb_2O_3 to ZnO-MnO_2-Bi_2O_3-TiO_2-Co_2O_3-based ceramic varistors improves the electrical properties. Small amounts of Sb_2O_3 and/or Cr_2O_3 limit ZnO grain growth and may affect the electrical properties.

2. Experimental

The powder was prepared using the mixed oxide method in alcoholic medium. All the oxides used were analytical grade: ZnO, MnO_2, Bi_2O_3, TiO_2 ,Cr_2O_3 and Sb_2O_3. The molar compositions of the investigated systems were as shown in Table 1. The amounts of Bi_2O_3 , Co_2O_3 and TiO_2 were always kept constant, because these additives were used to facilitate densification during sintering. In this study, these compositions were chosen to evaluate the phenomena involved on the physical and electrical properties of this varistor system. Two discs were used, the first one has 1.2 cm diameter and 0.2 cm thickness, and the second disc has 5 cm diameter and 0.2 cm thickness. These two discs were processed by a semi-dry press method under 70 KN. The pellets were sintered at (800 – 1220 ^{0}C) for 2 h in oxygen atmosphere and slowly cooled to room temperature (5 ^{0}C/min). The optimum firing temperature for each mix was deduced from the determination of the following parameters; firing shrinkage, apparent porosity, bulk density and water absorption. The method given is according to the ASTM standard (C71, C72) [36]. The different mixes were examined by XRD. Using Philips apparatus type 170, a vanadium (λ =1.54 Å) and Ni-filter. In Metallurgy Research Center, Egypt. A continuous plot of intensity for 2θ values 4 to 80 was made at a scanning speed of 1^o / min, with a paper speed of 10 mm/min. Mean grain size was determined by analyzing the SEM micrographies (Joel-JEM. T 200). To perform the electrical measurements, silver contacts were deposited on the sample surfaces. The (I-V) measurements of these samples were made by using a DC power supply in a current range up to 2 mA and pulse technique (8×20 μs current pulses) for higher current ranges as described elsewhere . The non-linearity index (α) was calculated in a current range of 1 mA to 1 A using the following equation:

$$\alpha = (\text{Log } I_2 - \text{Log } I_1) / (\text{Log } V_2 - V_1)$$

Where I_1 and I_2 are the currents at the voltages V_1 and V_2. The connection of varistors sample in electric circuit is show in Fig. 1.

The PM 6304 programmable automatic RCL meter was used for precise measurements of resistance, capacitance and inductance. From the measured values of capacitance, the dielectric constant at all frequency from 1 KHz- 200 KHz was calculated at constant temperature. The respective permittivity [ξ] and conductivity [σ] were calculated according to the following relations: $\epsilon' = \frac{C\,d}{\epsilon_o\,A}$, where C = capacitance in Farad., d = thickness of specimen in m., ϵ_o = dielectric constant of vacuum 8.85 ×10^{-12} F/m., A = area of specimen in m^2. Also from the values of resistance [R], the resistivity [ρ] and conductivity [σ] were calculated from the following relation: Resistivity **[ρ]** = $\frac{R\,A}{d}$, Where R: resistance, d = thickness of specimen in m., A = area of specimen in m^2.

Table 1. Composition of different mixes in mol %

Oxides	ZnO	MnO_2	Bi_2O_3	Co_3O_4	Ti_2O_3	Cr_2O_3	Sb_2O_3
B1	**97.56**	**0.5**	**0.7**	**0.5**	**0.7**	**0.04**	**---**
B2	**97.48**	**0.5**	**0.7**	**0.5**	**0.7**	**0.12**	**---**
B3	**97.40**	**0.5**	**0.7**	**0.5**	**0.7**	**0.20**	**---**
Z1	**98.06**	**0.5**	**0.7**	**0.5**	**-**	**0.12**	**0.12**
Z2	**98.12**	**0.5**	**0.7**	**0.5**	**-**	**0.06**	**0.12**

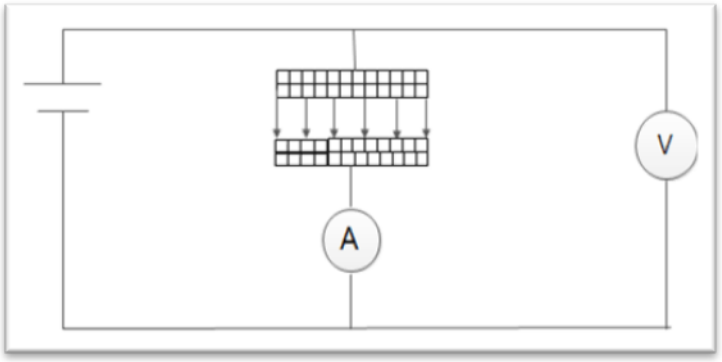

Fig. 1. The position of varistor sample in electric circuit

Results and Discussion:

Minimum water absorption appear in samples (B2) and (Z1) equal to 1.088 and 1.153, fired at 1220 ^{o}C for 2 hours, respectively. It is evident that better densification and less water absorption are achieved in all mixes fired at 1220 ^{o}C for 2 hours as shown in Figs. 2 and 3. Therefore, this temperature was the selected as the proper maturing temperature for all mixes. Above 1220 ^{o}C all samples were start of deformation. Water absorption of mixes Z1 and Z2 is less than mixes B1, B2 & B3, i.e. addition of Sb_2O_3 in present of Co_2O_3, MnO_2, Sb_2O_3 and Cr_2O_3 lead to better densification by minimizing the present of closed pores. Results of firing shrinkage as a function of temperature of different are graphically plotted in Figs. 4 and 5, showed increase of shrinkage with rise in temperature. Maximum values of firing shrinkage were attained in specimens fired at 1220 ^{o}C for 2 hours. Higher sintering temperature and longer sintering times give rise to a reduction in bulk densities due to increased amount of porosity between the large grains of ZnO resulting from the rapid grain growth induced by the liquid phase sintering and also the Bi_2O_3 losses especially in sintering above 1220 ^{o}C.

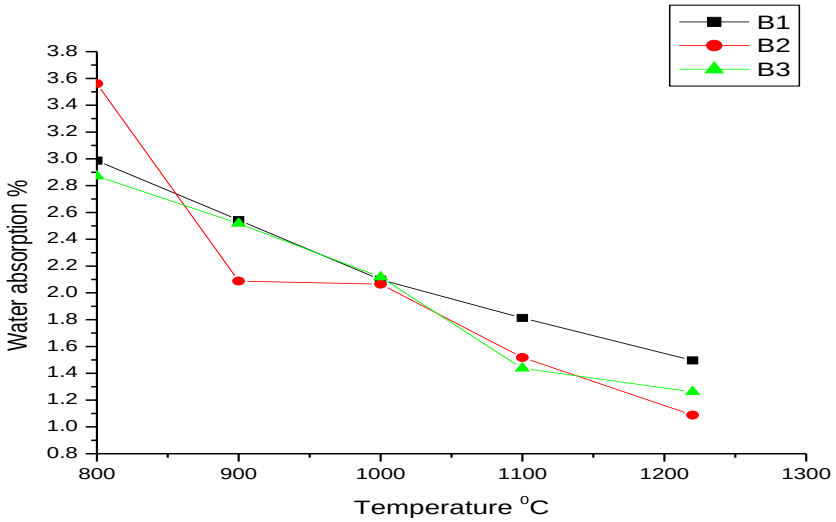

Fig. 2. Water absorption of mixesB1,B2&B3

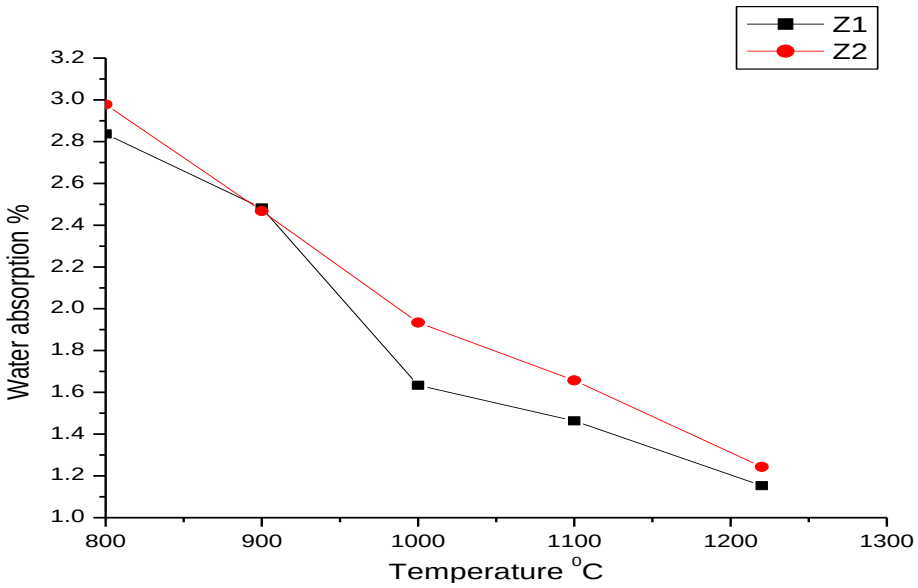

Fig. 3. Water absorption of mixes Z1&Z2

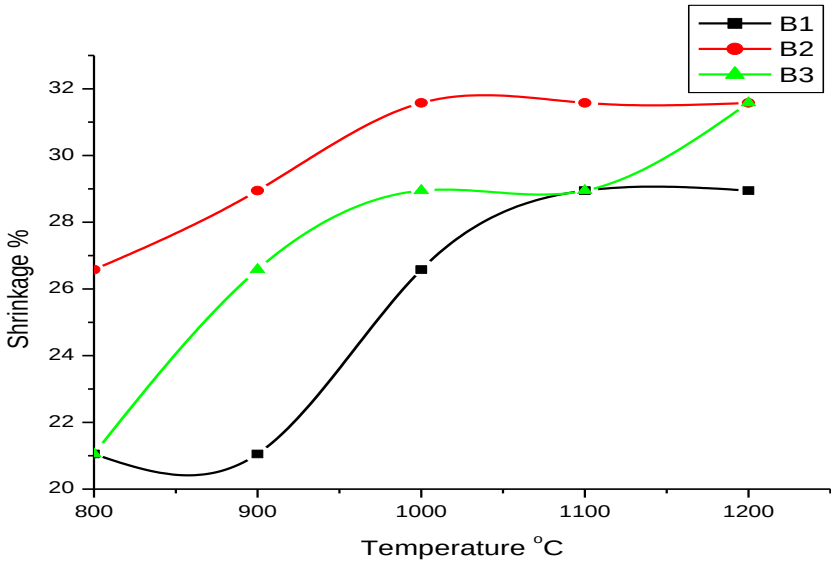

Fig. (4): Firing % shrinkage of B, B2 and B3

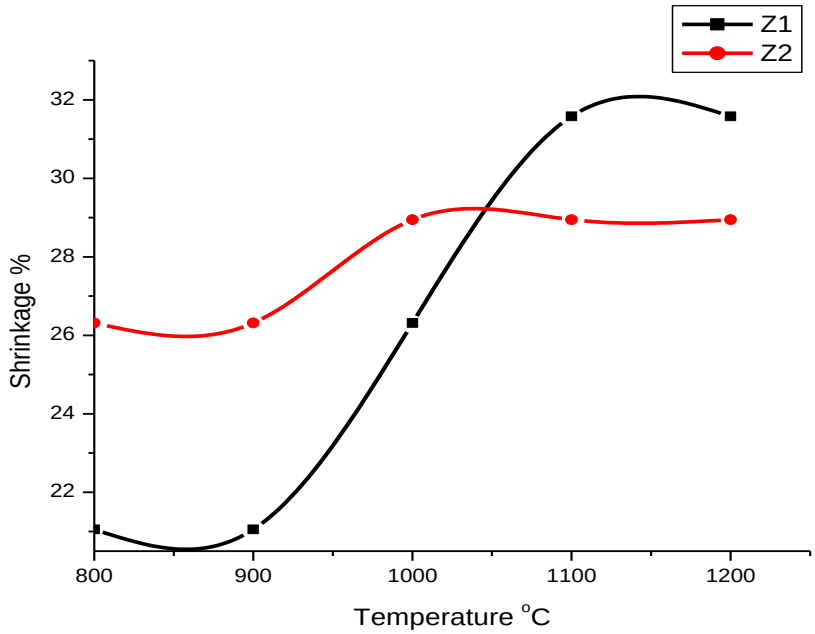

Fig. (5): Firing % shrinkage of samples Z1and Z2

Fig. 6. show the X-ray diffraction patterns of different mixes, namely (B_1, B_2 and B_3),which containing ZnO, Bi_2O3, TiO_2, Co_3O_4, MnO_2 and Cr_2O_3. XRD patterns of sample (B_1) , in which ZnO diffraction can be detected at about 2θ = 36.356 (d = 2.46912 Å), 47.647 (d = 1.90706 Å) and 56.666 (1.62307 Å), hexagonal structure, the lattice constants are a = b = 3.24880 and c = 5.2054 (PDF number is (186)-2-47.5807). Hausmannite Mn_3O_4 can be detected at about 2θ = 28.93 (d = 3.08386 Å), 2θ = 32.579 (d = 2.74628 Å), tetragonal structure, the lattice constants are a = b = 5.76500 and c = 9.44200 (PDF number is (141)-4-313.807). Anatase TiO_2 can be observed at about 2θ = 29.496 (d = 3.02590 Å) and 34.537 (d = 2.59495 Å), tetragonal structure, the lattice constants are a = b = 3.80400 and c = 9.61400 (PDF number is (141)-4-139.119). XRD patterns of sample (B_2), in which ZnO can be diffraction detected at about 2θ = 31.809 (d = 2.81096 Å), 34.465 (d = 2.60019 Å), 36.287 (d = 2.47365 Å), 47.595 (d = 1.90902 Å) and 56.648 (1.62354 Å), hexagonal structure, the lattice constants are a = b= 3.2488 and c = 5.2054 (PDF number is (186)-2-47.5807). Also, Hausmannite Mn_3O_4 can be detected at about 2θ = 28.891 (d = 3.08792 Å) and 2θ = 32.562(d = 2.74768 Å), tetragonal structure, the lattice constants are a = b = 5.76500 and c = 9.44200 (PDF number is (141)-4-313.807). Zinc Antimony oxide ($Zn_7Sb_2O_{12}$) can be detected at about 2θ = 34.465 (d = 2.60019 Å) and 77.021(d = 1.23712 Å), cubic structure, the lattice constants are a = b = c = 8.59400 (PDF number is (227)-1-63). XRD patterns of sample (B_3), in which ZnO can be detected by the diffraction at about 2θ = 31.847 (d = 2.80966 Å), 2θ = 34.504 (d = 2.59735 Å), 2θ = 36.324 (d = 2.47123 Å), 2θ = 47.61 (d = 1.90846 Å), 2θ = 56.636 (d = 1.62387 Å), hexagonal structure, the lattice constants are a = b = 3.24900 and c = 5.2052 (PDF number is (186)-2-47.587). Valentitnite Sb_2O_3 can be detected at about 2θ = 29.389 (d = 3.066 Å), 2θ = 46.698 (d = 1.94357 Å), orthorhombic structure, the lattice constants are a = 4.92, b = 12.46, c = 5.62 (PDF number is (56)-4-344.524).
Zinc Antimony oxide ($Zn_7Sb_2O_{12}$) can be detected at about 2θ = 72.619 (d = 1.30086 Å), 2 θ = 76.985 (d = 1.23760 Å), cubic structure, the lattice constants are a = b = c = 8.59400 (PDF number is (227)-1-63). Fig. 7. shows the X-ray diffraction patterns mixes (Z_1, Z_2) which containing ZnO, Bi_2O3, Co_3O_4, MnO_2, Sb_2O_3 and Cr_2O_3. XRD patterns of sample (Z_1), in which ZnO can be detected by the diffraction at about 2θ = 32.008 (d = 2.79393 Å), 2θ = 34.672 (d = 2.58513 Å), 2θ = 36.496 (2.45997 Å), 2θ = 47.774 (d = 1.90230 Å), 2θ = 56.802 (d = 1.61950 Å) 2θ = 63.044 (1.47334 Å), hexagonal structure, the lattice constants of ZnO are a = b = 3.24170 and c = 5.18760 (PDF number is (186)-2-47.2110). Bismuth cobalt oxide, can be detected at about 2θ = 27.943 (d = 3.19049 Å), 2θ = 32.826 (d = 2.72616 Å), tetragonal structure. The lattice constants are a = b = 7.7314 and c = 5.6361. Zinc Antimony oxide ($ZnSb_2O_4$) can be detected at about 2θ = 27.943 (d = 3.19049 Å), 2θ = 29.538 (d = 3.02169 Å),
2θ = 72.778 (d = 1.2984 Å), 2 θ = 63.26 (d = 1.46883 Å), tetragonal structure, the lattice constants are a = b = 8.94090 and c = 5.9197 (PDF number is (135)-4-426.783). Zinc Antimony oxide ($Zn_7Sb_2O_{12}$) can be detected at about 2θ = 29.538 (d = 1.97517 Å), 2θ = 72.778 (d = 1.29841 Å), cubic structure, the lattice constants are a = b = c = 8.59400 (PDF number is (227)-1-63). XRD patterns of sample (Z2), in which ZnO can be detected by the

diffraction at about 2θ = 31.901 (d = 2.80302 Å), 2θ = 34.576 (d = 2.59211 Å), 2θ = 36.393 (2.46673 Å), 2θ = 47.671 (d = 1.90614 Å), 2θ = 56.702 (d = 1.62211Å) 2θ = 63.18 (1.47049 Å), hexagonal structure, the lattice constants of ZnO are a = b = 3.24170 and c = 5.18760 (PDF number is (186)-2-47.2110). Bismuth cobalt oxide , can be detected at about 2θ = 27.853 (d = 3.20053 Å), 2θ = 47.671 (d = 2.98540 Å), tetragonal structure, the lattice constants are a = b = 7.7314 and c =5.6361. Zinc Antimony oxide ($ZnSb_2O_4$) can be detected at about 2θ = 27.853(d = 3.2005 Å), 2θ = 29.905(d = 2.98540 Å), 2 θ = 62.979 (d = 1.47470 Å), tetragonal structure, The lattice constants are a = b = 8.94090 and c = 5.9197 (PDF number is (135)-4-426.78). Zinc Antimony oxide ($Zn_7Sb_2O_{12}$) can be detected at about 2θ = 29.41 (d = 3.03458 Å), 2θ = 34.576 (d = 2.59211 Å), cubic structure, the lattice constants are a = b = c = 8.59400.

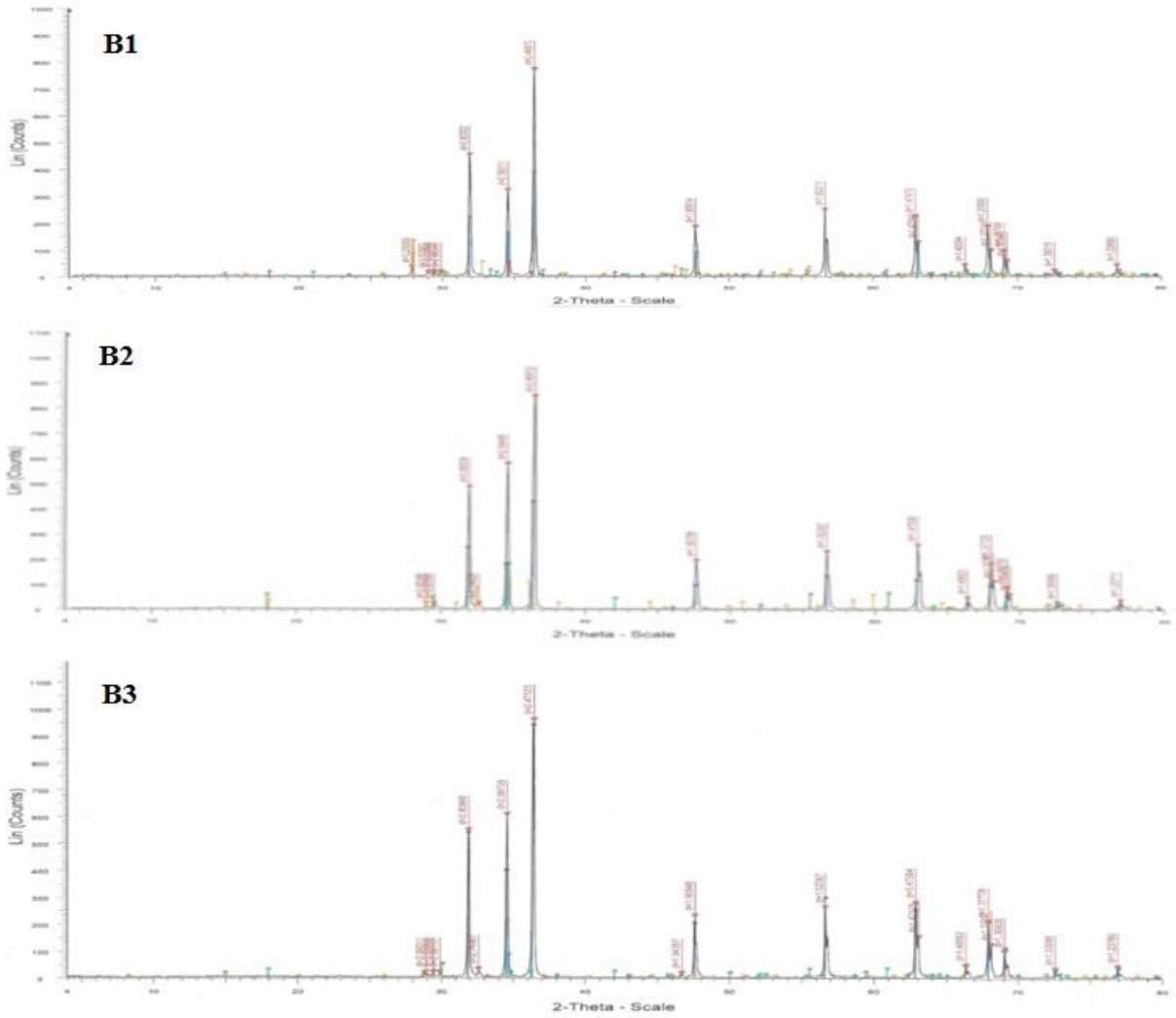

Fig. 6. XRD of mixes B1,B2&B3

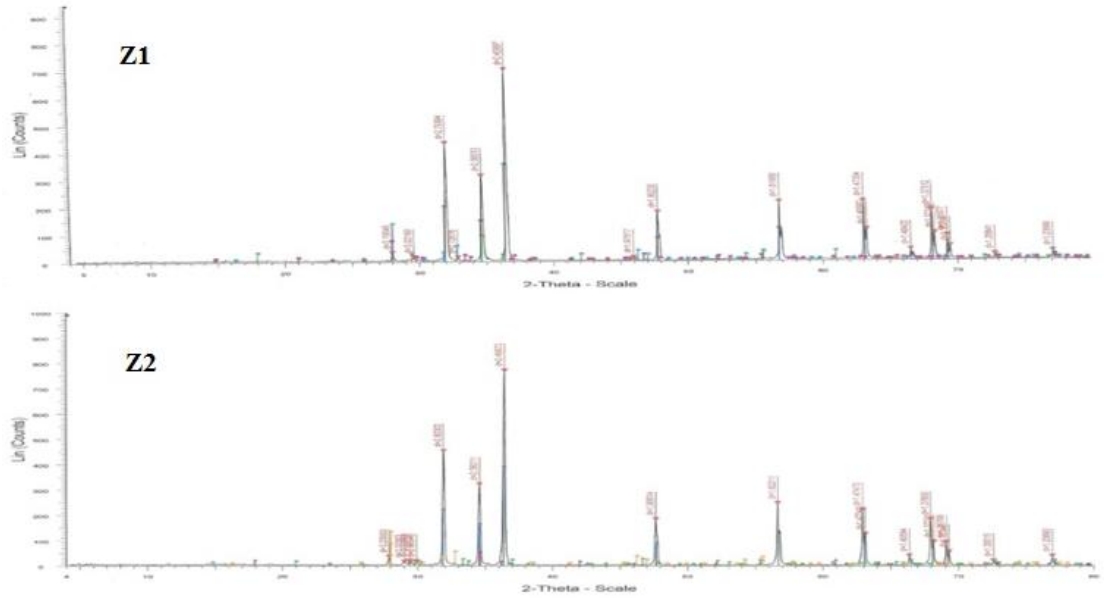

Fig. 7. XRD of mixes Z1&Z2

., SEM of mix B1, Fig. 8, shows two phases, ZnO grains and intergranular phase triple point, also TiO_2, Co_2O_3 and Cr_2O_3 go into solid solution in the ZnO grains also Bi-rich phase in the triple point and increase the presence of liquid phase (melt liquid phase) on the grain boundary. Fig .9. SEM of mix B2, shows different phase of ZnO grain, the exsolution of Bi-rich phase along the grain boundary, in various size. SEM of mix Z2 present in Fig. 10. shows the presence of a spinal phase between ZnO and Sb_2O_3 ($Zn_7Sb_2O_{12}$), intergranular layers, a Bi-rich phase, and triple points. During first stage of the sintering heterogeneous reactions from the powder particles lead to spinal phases [37] as shown in the following equations:

$$\mathbf{ZnO + Sb_2O_3 + O_2 \longrightarrow ZnSb_2O_6.}$$

$$\mathbf{ZnSb_2O_6 + 6ZnO \longrightarrow (\alpha)Zn_7Sb_2O_{12}}$$

In a second stage a low melting point eutectic between ZnO, Bi_2O_3 and Sb_2O_3 is formed above 700 ^oC. The third stage, liquid phase densification at the sintering temperature is the step where the main ZnO grain growth occurs. At this temperature the ZnO grain are still small but tend to grow with the temperature despite the presence of spinal phases which hinder ion transfer. As a result the grain growth is limited by pinning migrating ZnO grain boundaries. Another reaction leads to the pyrochlore phase ($Zn_2Bi_3Sb_3O_{14}$) formation which is rather unstable and decomposes during the early stage of sintering by solid-state reaction of ZnO with pyrochlore ($Zn_2Bi_3Sb_3O_{14}$) according to ref [38]:

$$\mathbf{2Zn_2Bi_3Sb_3O_{14} + 17\ ZnO \longrightarrow 3(\beta)Zn_7Sb_2O_{12} + 3Bi_2O_3}$$

Which gets free liquid Bi_2O_3-rich phase above 950 ^oC. During cooling, Bi-rich phase recedes to multigrain junctions. This operation is critical since extra bismuth concentration is rather detrimental to produce good varistor electrical properties [39,40]. The spinal phases, embedded in the liquid phase, are expelled to the multi-junctions. This creates a microstructure constituted of ZnO grains where the space at multiple-grain junctions and partially surrounding ZnO grains are filled by bismuth rich phase.

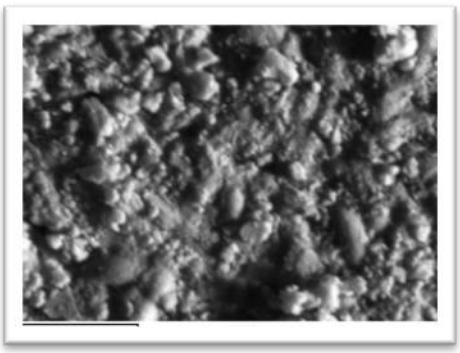

Fig. 8. SEM of mix B_1 , thermally etched X=3000.

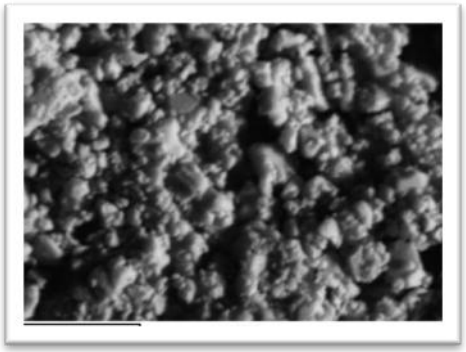

Fig. 9. SEM of mix B_2 ,thermally etched, X=3000.

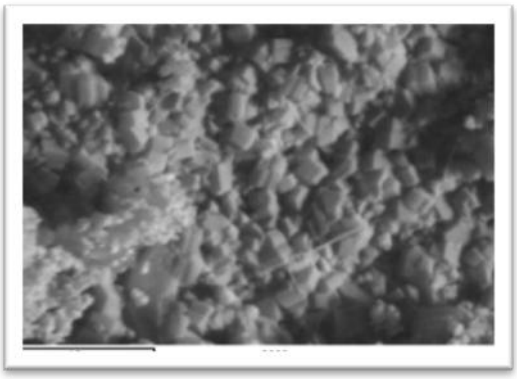

a

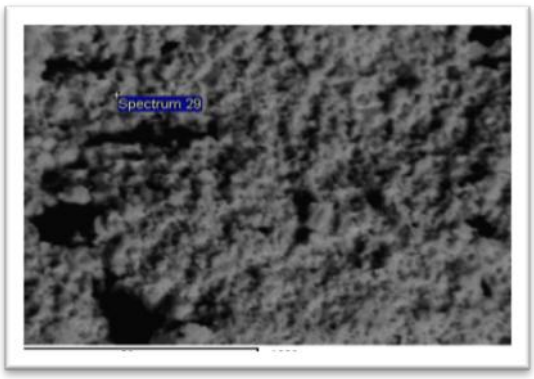

b

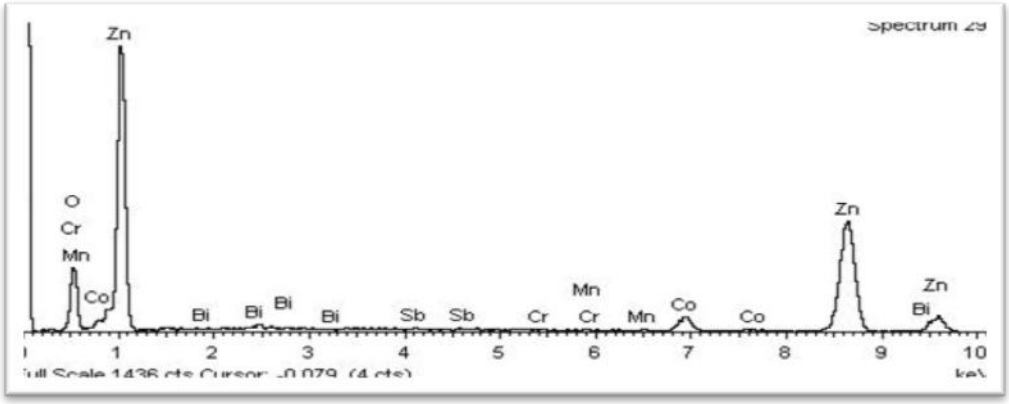

(c)

Fig. 10 SEM and XRD of mix Z_2, (a) thermally etched, ZnO grains in preferred orientation. (b) Thermally etched, of mix Z_2 shows the random distribution of minor elements. (c) EDAX of Z2, shows the concentration of Bi_2O_3, Sb_2O_3, Cr_2O_3, MnO_2 with ZnO and Co_3O_4 in intergranular.

The relation between I and V for the different mixes show very good plateau in (I-V) relation which are present in Figs. (11,12). The characteristic curves of different groups are greatly divided into two regions, that is pre break down at low voltage region and an off-state and nonlinear properties as an on-state high voltage region, the sharper the knee of the curves between the two regions, the better the nonlinearity. The non-linear behavior in ZnO-base materials is attributed to the formation of interface states in the band gap of ZnO which lead to the development of potential barriers to electrical conduction at ZnO grain boundaries. Although the intrinsic defects of zinc oxide can account themselves for the formation of such potential barriers in pure ZnO [41], the presence of external dopants

located both at the grain boundaries and inside the grains is expected to alter the local configuration, so affecting the non-linear behavior of the system.

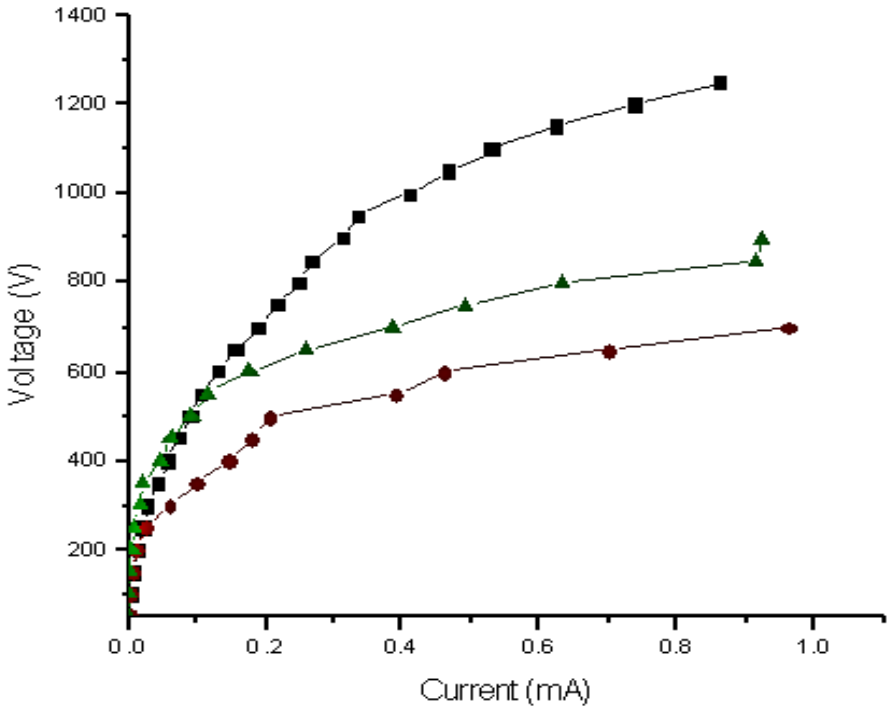

Fig. 11. I-V Characteristics of mixes B1 (■), B2 (●) and B3 (▲).

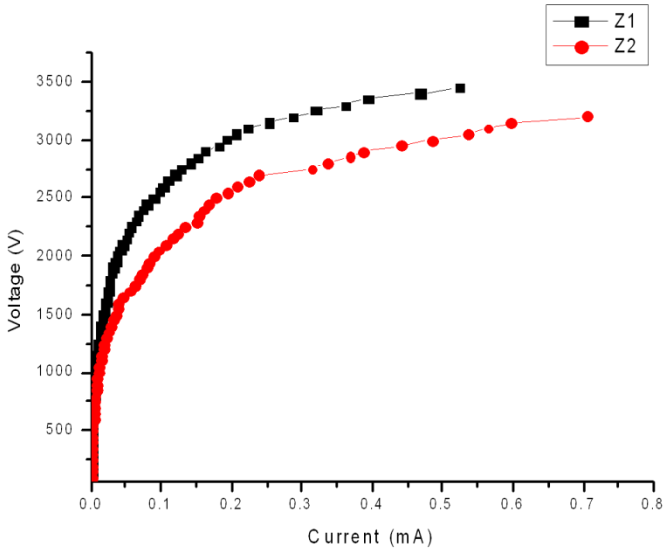

Fig. 12. I-V Characteristics of mixes Z1 and Z2

The results of dielectric constant as a function of frequency at room temperature of different mixes are graphically plotted in Figs. (13 and 14). A decrease in capacitance and consequently in dielectric constants for different mixes was observed. This may be explained in the light of microstructure formed of semi-conductive ZnO grains surrounded by insulating glassy phase which is similar to that of grain boundary layer capacitors as a result the

observed dielectric constant increased with increase in dopant oxides. The relation between resistivity and frequency for the different mixes present

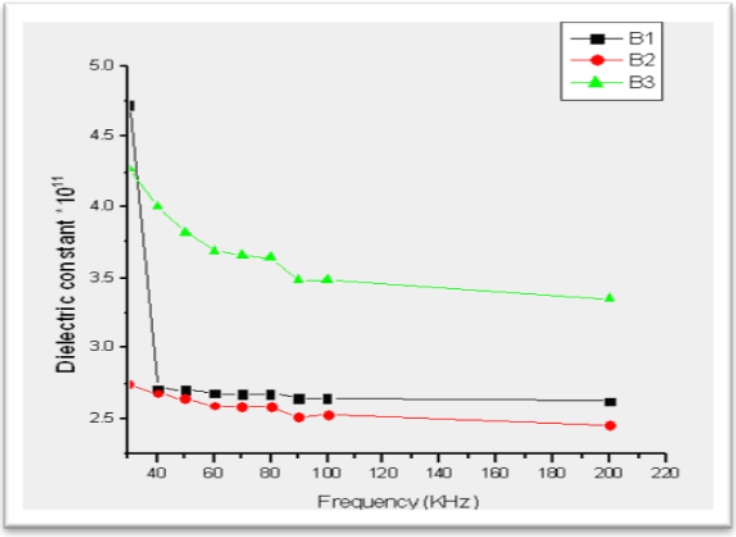

Fig.13.Dielectric constant as function of frequency of mixes B1,B2&B3

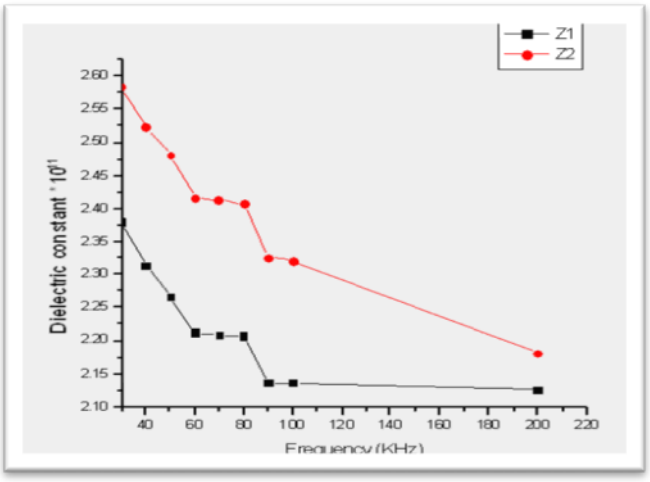

Fig.14.Dielectric constant as function frequency of mixes Z1&Z2

The relation between conductivity and frequency for different mixes are shown in Figs. (15,16). The conductivity increases with increasing frequency at room temperature. This may be attributed to the increase in the number of dipoles. The increase of frequency raised the conductivity because it increases the ionic response to the field again this is related to intergranular material at the field again this is related to intergranular material at any particular temperature. These effect are associated with polarization currents arising from trapping states of various kinds and densities. The increase in frequency raised the conductivity as a result of the increase in ionic response to the field again this is related to inter-granular material.

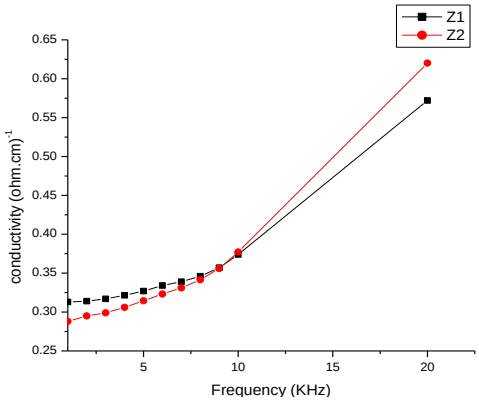

Fig. 15.AC Conductivity as a function of frequency of mixes Z1 and Z2

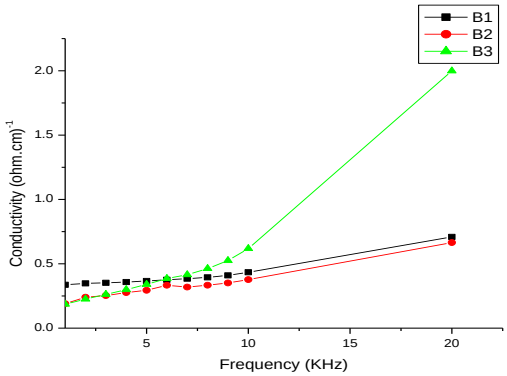

Fig. 16. AC Conductivity as a function of frequency of mixes B1,B2and B3

References

[1] D C. Look 2001 Mater. Sci. Eng. B 80 ,383
[2] U Ozg¨ur, Y I Alivov, C Liu, A Teke, M A Reshchikov, S Dogan, VAvrutin, S-J Cho and H Morkoc¸ 2005 J. Appl. Phys. 98**,** 041301
[3] S B Ogale 2005 Thin Films and Heterostructures for Oxide Electronics (New York: Springer)
[4] H N Nickel and E (ed) Terukov 2005 Zinc Oxide- A Material for Micro- and Optoelectronic Applications (Netherlands: Springer)
[5] C Jagadish and S J (ed) Pearton 2006 Zinc Oxide Bulk, Thin Films, and Nanostructures (New York: Elsevier)
[6] D G Thomas 1960 J. Phys. Chem. Solids **15 ,**86
[7]A Mang ,K Reimann and St R¨ubenacke 1995 Solid State Commun. **94,** 251
[8]D C Reynolds ,D C, Look, B Jogai B, CW Litton, G Cantwell and W C Harsch 1999 Phys. Rev. B **60,** 2340
[9] Chen Y, Bagnall D M, Koh H-J, Park K-T, Hiraga K, Zhu Z-Q and Yao T 1998 J. Appl. Phys. **84,** 3912
[10] V Srikant and D R Clarke 1998 J. Appl. Phys. **83 ,**5447
[11] D C Reynolds , D C Look and B Jogai 1996 Solid State Commun. **99,** 873
[12] D M Bagnall D M, Y F Chen,Z Zhu, T Yao, S Koyama, M Y Shen and T Goto 1997 Appl. Phys. Lett. **70** ,2230
[13] M E (ed) Brown 1957 ZnO—Rediscovered (New York: The New Jersey Zinc Company)
[14] K. Al Abdullah, M.D. l Termanini, F.Alhaj OmarLHAJ Omar Energy Procedia 18 (2012) 867 – 878
[15] F.A. Krfger 1974 The Chemistry of Imperfect Crystals, North-Holland, Amsterdam, 743.
[16] M.H. Sukkar, H.L. Tuller1983 Defect equilibria in ZnO varistor materials, in: M.F. Yan, A.H. Heuer (Eds.), Advances in Ceramics, vol. 7, The American Ceramic Society, , p. 71.
[17] J. Han, P. Mantas, A.M.R. Senos 2002 J. Eur. Ceram. Soc. 22,49.
[18] L. Harry, Tuller, 1999 J. Electroceram. 4 , 33
[19] E. Olsson, G. Dunlop, R. Osterund 1993 , J. Am. Ceram. Soc. 76 , 65.
[20] T.K. Gupta, W.D. Straub1990 , J. Appl. Phys. 68 , 845.
[21] F. Greuter, G. Blatter 1990 Semicond. Sci. Technol. 5 , 111.
[22] H.A. Harwig, A.G. Gerrards1978 J. Solid State Chem. 26 , 265.
[23] J. Wong 1974 , J. Am. Ceram. Soc. 57 , 357.
[24] J. Kim, T. Kimura, T. Yamaguchi, 1989 J. Am. Ceram. Soc. 72 , 1390
[25] P. Dura´n, F. Capel, J. Tartaj, C. Moure 2001 , J. Am. Ceram. Soc. 84, 1661.
[26] A. Iga, M. Matsuoka, T. Masuyama 1976 Jpn. J. Appl. Phys. 15 ,1161.
[27] J. Wong, W.G. Morris1974 , Ceram. Bull. 53 , 816.
[28] N. Daneu, A. Rae`nik, S. Bernik, D. Kolar 2000 J. Am. Ceram. Soc. 83 , 3165.
[29] E. Olsson, G.L. Dunlop, R. O¨ sterlund, J. Appl. Phys. 66 (1989) 5072.
[30] E. Olsson, L.K.L. Falk, G.L. Dunlop, R. Osterlund,1985 J. Mater. Sci. 20 4091.
[31] L.M. Levinson, H.R. Philip1975 , J. Appl. Phys. 46 , 1332.
[32] W.G. Morris1973 , J. Am. Ceram. Soc. 56 , 360.
[33] L.M. Levinson, H.R. Philipp 1986 Zinc oxide varistor — a review, Ceram. Bull. 65 (4), 639 .
[34] T.K. Gupta1990 Application of zinc oxide varistor, J. Am. Ceram. Soc. 73 (7) , 1817.

[35] S.A. Pianaro, P.R. Bueno, E. Longo, J.A. Varela 1999, Microstructure and electric properties of a SnO2 based varistor, Ceram. Int. 25 , 1.
[36] Alnual book of ASTM standards, American society for testing and material, 1966**.**
[37] M. Inada 1979, Jpn. J. Appl. Phys., 18, 1439-1446 .
[38] M. Inada1980, Jpn. J. Appl. Phys., 19, 409.
[39] K. I. Kobayashi, O. Wada, M.Kobayashi, Y. Takada1998 , J. Am. Ceram. Soc., 81, 2071.
[40] T. Asokan1987 , Br. Ceram. Trans. J., 80, 187.
[41] V. Srikant, V. Sergo, and D. R. Clarke1995 , J. Am. Ceram. Soc., 78, 1935.